AIAA 2013-2279

Acoustic field associated with parabolized stability equation models in turbulent jets

Daniel Rodríguez[1,2]*, Aniruddha Sinha[1]†, Guillaume A. Brès[3]‡ and Tim Colonius[1]§

[1] *California Institute of Technology, Pasadena, CA*

[2] *School of Aeronautics, Universidad Politécnica de Madrid, Spain*

[3] *Cascade Technologies Inc. Palo Alto, CA*

Wavepackets are large-scale turbulent structures that are correlated and advected over distances that are large compared to the integral scales of turbulence, and have been shown to be responsible for the peak noise radiated at aft angles to the jet axis. The present paper discusses linear models of these wavepackets for supersonic turbulent jets based on Parabolized Stability Equations (PSE). In the past, results of this approach were shown to be in excellent agreement with coherent structures extracted from experimental near-field pressure and velocity data in subsonic jets. Here, we make use of a Large Eddy Simulation (LES) database for an isothermal and a moderately heated Mach 1.5 turbulent jets. Careful comparisons of the PSE models with near-field pressure fields from LES, filtered by means of Proper Orthogonal Decomposition (POD), demonstrate acceptable fidelity of the model. Finally, the acoustic far-field associated with the PSE wavepackets is computed using a Kirchhoff surface method, capturing reasonably well the far-field pressure at angles close to the peak.

I. Introduction

Jet noise and its reduction is a technological problem of great importance that has received continuous attention for decades. State-of-the-art numerical simulations are today capable of predicting simultaneously the turbulent mixing flow and the noise radiated thereof with remarkable accuracy. On the other hand, the understanding of the physics involved in the generation of turbulent mixing noise and reduced-order models for its prediction and control are lacking. The peak noise radiation in the aft direction has been linked to the dynamics of the large-scale structures observed in turbulent jets.[1] These structures, intermittent advected wavepackets that correlate over spatial distances far exceeding the characteristic scales of turbulence, are related to, and have been modeled by instability waves.[2–4] In addition, evidence has been amassed that the noise radiated to the acoustic far-field is mostly contained in the first few azimuthal wavenumbers and lower frequencies. Under these conditions, the wavepackets are most coherent along the axial direction becoming most efficient sound radiators and thus dominating the acoustic far-field in spite of their relatively low kinetic energy. Over the last decades, a theory based on the existence and dynamics of wavepackets as the prominent noise sources has been elaborated, and extensive comparisons with data from simulations and experiments have demonstrated its utility.[5]

Theories modeling wavepackets as instability waves of the turbulent mean flow were discussed by Crighton and Gaster.[6] Most of these attempts consider statistical descriptions of the wavepackets in the frequency domain, permitting the derivation of a set of equations describing the evolution of individual frequency and azimuthal modes, while nonlinear interactions between modes appear as Reynolds stresses. As opposed to laminar and transitional flows, when turbulent flows in statistical equilibrium are considered, the structures

*Marie Curie COFUND fellow. Present address: Escola de Engenharia de São Carlos, Universidade de São Paulo, Brazil. AIAA Member. dani@torroja.dmt.upm.es

†Postdoctoral Scholar, Department of Mechanical Engineering. AIAA Member.

‡Senior Research Scientist. AIAA Member.

§Professor, Department of Mechanical Engineering. AIAA Associate Fellow.

corresponding to lower frequencies and azimuthal wavenumbers have relatively small energy, and the nonlinear interactions between them may be negligible, insofar as their average evolution in the turbulent mean flow. Nonlinearity inherent in the turbulent mixing is accounted for in the establishment of the mean flow. A step beyond the use of parallel-flow and multiple-scales stability theories in the modeling of the wavepackets is achieved with the introduction of the Parabolized Stability Equations (PSE).[7–13] PSE takes into account the mild divergence of the jet mean flow along the axial direction, and also permits the introduction of nonlinear interactions between the different frequency and azimuthal wavenumbers.[14] Further improvements can be achieved with the introduction of *ad hoc* eddy viscosity models.[15,16]

The approach of using linear instability waves in the wavepacket modeling has been widely employed in the study of *forced* supersonic jets,[2,15,17,18] for which the measured near-field fluctuations were found to be in good agreement with the predictions of linear stability theory.[19] In the case of *subsonic natural* jets, this approach has only recently begun to deliver satisfactory quantitative predictions. One of the difficulties associated with the experimental observation of the coherent structures in natural jets is the lack of a phase reference, that is trivially determined in forced jets. Advanced measurement techniques and post-processing techniques are consequently required in order to detect the physical wavepackets within the flow field. Suzuki and Colonius[20] considered a series of measurements performed at the NASA Glenn SHJAR facility, in which a microphone phased-array was placed outside of the turbulent mixing-layer, in a region where hydrodynamic fluctuations are expected to behave linearly and the importance of acoustic fluctuations to be small. The careful location of the array and the high-quality measurements were instrumental in demonstrating that the pressure fluctuations measured just outside of the jet shear layer were consistent with the evolution of linear instability waves computed using locally parallel flow analysis of the jet mean flow. In Gudmundsson and Colonius,[13] Proper Orthogonal Decomposition (POD)[21,22] was applied to the same measurements in order to filter out the part of the pressure fluctuations that were uncorrelated over the microphone array, resulting in remarkable comparisons with the solutions of linear PSE. Recently, Particle Image Velocimetry (PIV) measurements performed at cross-sections along with POD were also employed to extract the coherent structures from the total turbulent field showing that linear instability waves also compare well with the large-scale fluctuations in the velocity field.[23]

Once sufficient evidence is obtained that the instability wave models can successfully reproduce the most salient features of the physical wavepackets, they can be employed as noise source models in acoustic projection methods with the final objective of predicting the noise emitted by these structures to the far field. Techniques based on Lighthill's acoustic analogy[24] are commonly towards this.[12,25–27] On the other hand, Kirchhoff surface methods can, in principle, be used in order to directly project the modeled near-field pressure to the far field.[1,8,10,28,29] However, it is presently unclear if the fidelity of the PSE models is good enough to yield accurate far-field predictions via either Lighthill or Kirchhoff methods.

The present work considers *supersonic* unforced turbulent jets. Following previous experience in subsonic jets,[13,23] linear PSE is used to model the evolution of wavepackets and a Kirchhoff surface method is used to compute their acoustic far field. The model is applied to two ideally-expanded supersonic jets, one isothermal and one moderately heated, for which Large Eddy Simulation (LES) databases are available. The simulations were performed using the Cascade Technologies flow solver "Charles", and were designed to mimic the conditions in experiments performed at United Technologies Research Center (UTRC) facility.[30] Special attention was paid to converge the low-frequency spectra associated with the wavepackets, which requires much longer simulation times than the first and second-order statistics usually reported in analogous simulations. The databases were extensively validated against the experimental measurements.[31] The LES data is used here to extract the necessary input for the computation of PSE wavepacket models (i.e. the mean flow and fluctuations' amplitudes) and to perform a detailed evaluation of the modeling strategy. Quantitative comparisons are performed, showing very good agreement between the wavepacket signatures extracted from the LES databases and the PSE models both in the pressure near and far-fields, which constitutes the main novelty in the present contribution with respect to other works in the literature using the same modeling approach.[8,10]

II. Large Eddy Simulation database and processing

LES data corresponding to two supersonic jet configurations are used in the present work. The simulations consider ideally-expanded jets emanating from a convergent-divergent round nozzle with jet Mach number $M_j = U_j^*/c_j^* = 1.5$ at static temperature ratios $T_r = T_j^*/T_\infty^* = 1$ (isothermal) and $T_r = 1.74$

Table 1. Summary of operation conditions and jet parameters.

Case	Description	M_j	M_a	T_r	Re	$t_{\text{tot}}c^*_\infty/D^*$
B118	isothermal ideally-expanded	1.5	1.5	1	300,000	215
B122	heated ideally-expanded	1.5	1.98	1.74	155,000	112

(heated), respectively referred to as B118 and B122.[32] The subscripts j refer to the fully-expanded jet exit properties. The fluid surrounding the jet has a small co-flow component $\bar{u}_{co} = u^*_{co}/c^*_\infty = 0.1$ which is chosen to match the experimental conditions in the United Technologies Research Center (UTRC) anechoic facility.[30] The LES computations were performed using Cascade Technologies flow solver "Charles", on an unstructured mesh containing approximately 42 million control volumes. Extensive comparisons against measurements performed at UTRC, considering mean flow quantities and near and far-field pressure spectra, showed excellent agreement.[31]

Asterisks in the previous definitions denote dimensional quantities. In what follows, physical quantities are made dimensionless with the nozzle exit diameter D^*, the ambient density ρ^*_∞, and the ambient speed of sound c^*_∞. Besides this non-dimensionalization, some quantities are defined with variables different from the reference ones: the Reynolds number is based on the jet exit conditions: $Re = \rho^*_j U^*_j D^*/\mu^*_j$. The acoustic Mach number is defined as $M_a = U^*_j/c^*_j$. The dimensionless frequency used to show results will be the Strouhal number defined as $St = f^* D^*/U^*_j$. Table 1 summarizes the operation conditions of the two jet simulations.

Time-averaged mean flow variables were computed using the total simulation time (after initial transients) of $t_{\text{tot}} \approx 215 D^*/c^*_\infty$ for the B118 jet and $112 D^*/c^*_\infty$ for the heated jet, considered to be a long time sample of high-fidelity LES, thus ensuring the statistical convergence of the stationary quantities and also a reasonable convergence for the low-frequency noise spectra. In the computations of the discrete Fourier transforms in time used along this work, the time segments are extracted with a 75% overlap and a frequency bin $\Delta St = 0.025$, resulting in 29 segments for the B118 case and 19 segments for the B122.

In a previous work[33] we employed a database corresponding to the same B118 jet simulation in order to calibrate and validate the PSE wavepacket models. A spatial filter was applied to remove the small shock cells that appeared within the potential core, but this smoothing was subsequently determined to be too aggressive, imposing an artificial damping on the wavepackets. In addition, the time-dependent flow field variables were undersampled in spatial and temporal resolutions in order to deliver a reasonable-sized dataset, but the spatial resolution in the axial direction was found to be too coarse for the correct computation of the higher frequencies, while a very fine, but uniform, resolution was used on the radial direction. In the present paper, refined databases corresponding to the B118 and B122 jets are used. The ensemble-averaged mean field from LES is used without any spatial smoothing. The LES fluctuating data are interpolated to a structured cylindrical mesh with $N_x \times N_r \times N_\theta = 321 \times 176 \times 36$ points (where x, r, and θ are the axial, radial and azimuthal coordinates), resulting in a constant axial spacing of $\Delta x = 0.0625$ and a variable radial distribution with a minimum spacing $\Delta r = 0.01$ at the lipline and a maximum spacing $\Delta r = 0.1$ at the outer boundary. A constant time-step of $\Delta t = 0.02 D^*/c^*_\infty$ is also used in the extraction of the reduced database from the total LES simulation data.

III. Instability wave models

Parabolized Stability Equations (PSE) represent a generalization of the the parallel-flow linear stability theory (LST) for flows with a mild variation in the streamwise direction. Here, PSE are used as reduced-order model of the statistical wavepackets that are implicated in the peak mixing noise radiation; see Jordan and Colonius[5] for a recent review on the theoretical framework.

The turbulent flowfield is decomposed into a mean flow and temporal fluctuations, $\mathbf{q}(\mathbf{x}, t) = \bar{\mathbf{q}}(\mathbf{x}) + \mathbf{q}'(\mathbf{x}, t)$. In the present work, the mean flow is obtained directly from the time-average of the LES simulation. A cylindrical coordinate system is used where $\mathbf{x} = (x, r, \theta)$. The vector of fluid variables is $\mathbf{q} = [u_x, u_r, u_\theta, p, \zeta]$, where u_x, u_r and u_θ are the axial, radial and azimuthal velocity components, p is pressure and ζ is the specific volume, inverse of the density ρ. Assuming statistical stationarity of the mean flow quantities in time, and homogeneity along the azimuthal direction dictated by the round nozzle, the mean flow is only function of the axial and radial coordinates ($\bar{\mathbf{q}} = \bar{\mathbf{q}}(x, r)$) and Fourier modes are introduced for frequency

$\omega = 2\pi M_j St$ and wavenumber m following

$$\mathbf{q}'(\mathbf{x},t) = \sum_{\omega}\sum_{m} \breve{\mathbf{q}}_{\omega m}(x,r)\ \mathrm{e}^{\mathrm{i}m\theta}\mathrm{e}^{-\mathrm{i}\omega t} + \mathbf{q}''. \tag{1}$$

The unresolved fluctuations are formally gathered in the term $\mathbf{q}''$.

Owing to the slowly divergent nature of the mean flow along the axial direction, the fluctuations $\breve{\mathbf{q}}_{m,\omega}$ can be decomposed into a slowly-varying shape function (that evolves in the same $x-$scale as the mean flow) and a rapidly varying wave-like part:

$$\breve{\mathbf{q}}_{\omega m}(x,r) = A_{\omega m}(x)\ \tilde{\mathbf{q}}_{\omega m}(x,r) = A_{\omega m}(x_0)\exp\left(\mathrm{i}\int_x \alpha_{\omega m}(\xi)d\xi\right)\ \tilde{\mathbf{q}}_{\omega m}(x,r). \tag{2}$$

The axial wavenumber $\alpha_{\omega m}(x)$ is a complex quantity, for which a slow variation is also assumed. Note that the assumption of the existence of a single $\alpha_{\omega m}$ that describes the entire cross-stream variation implies that only a small portion of the fluctuations in a given Fourier mode pair (ω, m) is actually represented by $\breve{\mathbf{q}}_{\omega m}$, and the remaining is implicitly included in $\mathbf{q}''$.

Introducing this decomposition into the compressible Navier-Stokes, continuity and energy equations, and projecting them on to the retained Fourier basis, we arrive at the system of equations

$$\left(\mathbf{A} + \mathbf{B}\frac{d\alpha}{dx} + \mathbf{C}\frac{\partial}{\partial x} + \mathbf{D}\frac{\partial}{\partial r} + \mathbf{E}\frac{\partial^2}{\partial r^2} + \mathbf{F}\frac{\partial^2}{\partial x \partial r}\right)\tilde{\mathbf{q}}_{\omega m}(x,r) = \frac{\tilde{F}_{\omega m}}{A_{\omega m}} + \frac{F''_{\omega m}}{A_{\omega m}}. \tag{3}$$

The linear operators $\mathbf{A}$ to $\mathbf{E}$ are in general functions of the mean flow quantities, Reynolds number, Mach number, Prandtl number, frequency ω, azimuthal wavenumber m and axial wavenumber α. The right-hand-side contains nonlinear terms. The term $\tilde{F}_{\omega m}$ collects the quadratic interaction terms between the retained Fourier modes, and $F''_{\omega m}$ represents all other nonlinear terms. For unforced turbulent jets, the small relative amplitude of the individual modes suggests that nonlinear interactions between the lower modes can be neglected ($\tilde{F}_{\omega m}/A_{\omega m} \approx 0$). On the other hand, most of the nonlinearity related to the unresolved fluctuations is assumed here to be already accounted for with the use of the turbulent mean flow, and then $F''_{\omega m} \approx 0$.[6,15] Consequently, the right-hand-side is set equal to zero and linear PSE is used in what follows.

After spatial discretization of the radial direction, the system (3) can be rewritten as

$$\mathbf{L}\ \frac{\partial \tilde{\mathbf{q}}_{\omega m}}{\partial x} = \mathbf{R}\ \tilde{\mathbf{q}}_{\omega m} \tag{4}$$

where $\mathbf{L} = \mathbf{C} + \mathbf{F}\mathcal{D}_r$ and $\mathbf{R} = -(\mathbf{A} + \mathbf{B}\ d\alpha/dx + \mathbf{D}\mathcal{D}_r + \mathbf{E}\mathcal{D}_{rr})$ have been introduced. The matrix operators $\mathcal{D}_r$ and $\mathcal{D}_{rr}$ stand for the discrete versions of the first and second order spatial differentiation along the radial direction, respectively. Equation (4) is an initial value problem that can be integrated along the axial direction using an implicit Euler scheme. The explicit form of these operators, that depends on the discretization method employed and on the boundary conditions, is given elsewhere[13,33] along with details on the numerical solution.

The decomposition of (2) is ambiguous in that the spatial growth can be absorbed into the shape function $\tilde{\mathbf{q}}_{\omega m}$ or the complex amplitude $A_{\omega m}$. Following Herbert,[34] the normalization condition

$$\int_0^\infty \tilde{\mathbf{u}}^\dagger_{\omega m}\frac{\partial \tilde{\mathbf{u}}_{\omega m}}{\partial x}\ rdr = 0, \tag{5}$$

where $\tilde{\mathbf{u}}_{\omega m}$ refers to the three velocity components and $\dagger$ denotes complex conjugation, is imposed individually to every (ωm) mode, removing the exponential dependence from $\tilde{\mathbf{q}}_{\omega m}$.

Adequate conditions are required at the inlet x_0, specifically for $\tilde{\mathbf{q}}_{\omega m}(x_0,r)$, $\alpha_{\omega m}(x_0)$ and $A_{\omega m}(x_0)$. A local (i.e. for a fixed axial location) stability eigenvalue problem is solved in to determine the fluctuation profiles associated with the inviscid inflectional instability (or Kelvin-Helmholtz eigenmode), and these are used subsequently as the initial conditions in the linear PSE integration. In order to obtain the local stability problem based on the PSE (4), a further approximation is made assuming that the axial derivatives of the axial wavenumber and shape functions are also negligible, i.e.: $d\alpha_{\omega m}/dx \approx 0$ and $\partial\breve{\mathbf{q}}_{\omega m}/\partial x \approx \mathrm{i}\alpha_{\omega m}\breve{\mathbf{q}}_{\omega m}$. These assumptions are the same used in the derivation of usual local stability problems of the Orr-Sommerfeld kind, and result into the following matrix eigenvalue problem:

$$\mathrm{i}\alpha_{\omega m}\mathbf{L}\ \breve{\mathbf{q}}_{\omega m} = \mathbf{R}\ \breve{\mathbf{q}}_{\omega m}. \tag{6}$$

The linear operators $\mathbf{L}$ and $\mathbf{R}$ are the same as in (4), but particularized for $\alpha = 0$. In addition to the Kelvin-Helmholtz (K-H) eigenmode, there is a full eigenspectrum of solutions that is often ignored when computing initial conditions for the PSE integration, but is necessary in order to expand an arbitrary perturbation.[35,36] In our previous work,[33,37] we found that imposing the K-H eigenmode alone as the inlet condition delivered consistent wavepackets for the cold and moderately heated ideally-expanded jets of interest here.

IV. Comparison with LES near-field pressure

This section presents the PSE wavepacket models and compare them with the empirical wavepackets extracted from the LES databases for the isothermal and heated jets. The fluctuation pressure field in the turbulent mixing region and the near acoustic field are considered. Proper orthogonal decomposition (POD) of the LES flow field is used to filter the fluctuations most correlated over the PSE computational domain.

A. Extraction of wavepackets from LES data using proper orthogonal decomposition

The PSE models are intended to represent the coherent wavepacket motions at low frequencies and azimuthal wavenumbers. In order to validate these models with LES data, which resolves motions over a broad range of length and temporal scales, the wavepackets must be educed from LES using appropriate statistical techniques. Previous work considering subsonic jets employed POD to extract the signatures of flow structures which correlate over significant spatial regions, from either the pressure along a phased microphone array in the near-field[13] or velocity fluctuations at cross-sections measured using particle image velocimetry.[13,23]

The LES database used in the present research, in which all fluid variables are available on the full relevant flow domain, permits great flexibility in the computation of POD modes. A frequency-domain variant of Sirovich's snapshots method[38] is used here to decompose the two-dimensional structure of the (St, m) Fourier modes. In analogous manner to the PSE derivation, the LES data is Fourier-decomposed following

$$\breve{\mathbf{q}}^i(x, r; St, m) = \int_{t=0}^{2\pi/\omega} \int_{\theta=-\pi}^{\pi} \mathbf{q}'^i(x, r, \theta, t) \exp\left[\mathrm{i}\left(m\theta - 2\pi St M_j t\right)\right] \, dt d\theta. \tag{7}$$

Instead of performing a single Fourier transform using the total simulation time, several short-time Fourier transforms were computed for a given frequency bin ΔSt, as described in section II. The index i in (7) denotes the time segment used in the temporal Fourier transform.

A segment-to-segment cross-correlation matrix is defined now by applying an inner product to pairs of Fourier transformed perturbation fields, corresponding to different segments of data:

$$\breve{M}_{ij} = < \breve{\mathbf{q}}^i, \breve{\mathbf{q}}^j > \tag{8}$$

The use of different norms in the computation of POD modes of a turbulent jet was first done by Freund and Colonius,[39] showing that the resulting decomposition may be highly dependent on the physical variables of interest. The wavepackets are more readily apparent in the pressure field, and consequently the pertinent norm for POD is defined as

$$< \breve{\mathbf{q}}^i, \breve{\mathbf{q}}^k > = \int_x \int_r (\breve{p}^i)^\dagger \breve{p}^k \; r dr dx, \tag{9}$$

with † denoting complex conjugate. The integration is truncated here to the domain $0 \leq x \leq 20$, $0 \leq r \leq 5$, corresponding to the total domain of the extracted LES database.

POD modes are the optimal basis of orthogonal functions that minimizes the square mean error between the fluctuations $\breve{\mathbf{q}}^i$ and its projection on a basis of orthogonal functions. The l^{th} POD mode to be computed is retrieved as a weighted linear combination of the different transformed segments:

$$\breve{\phi}^l(x, r; \omega, m) = \sum_k \; \beta_k^l(\omega, m) \; \breve{\mathbf{q}}^k(x, r; \omega, m), \tag{10}$$

where the coefficients β_k^l are obtained as the eigenvectors of the eigenvalue problem

$$\breve{M} \; \beta^l = \sigma^l \; \beta^l. \tag{11}$$

The eigenvalues σ^l are real-valued and non-negative, and are arranged in descending order so that the first eigenvalue is the largest (the POD mode most representative of the fluctuating flowfield), the second corresponds to the second largest, and so on. The POD modes can be scaled to be directly comparable to the flow fluctuations as $\|\breve{\phi}^l(x,r;\omega,m)\| = \sqrt{\sigma^l}$, using the definition of the inner product in (9). To illustrate the relative importance of the respective POD modes, the eigenspectrum is usually normalized with the sum of all the eigenvalues, so that $\sum_l \sigma^l = 1$. A faster rate of decay of the σ^l series indicates a higher coherence of the LES data.

B. PSE wavepackets compared with POD modes

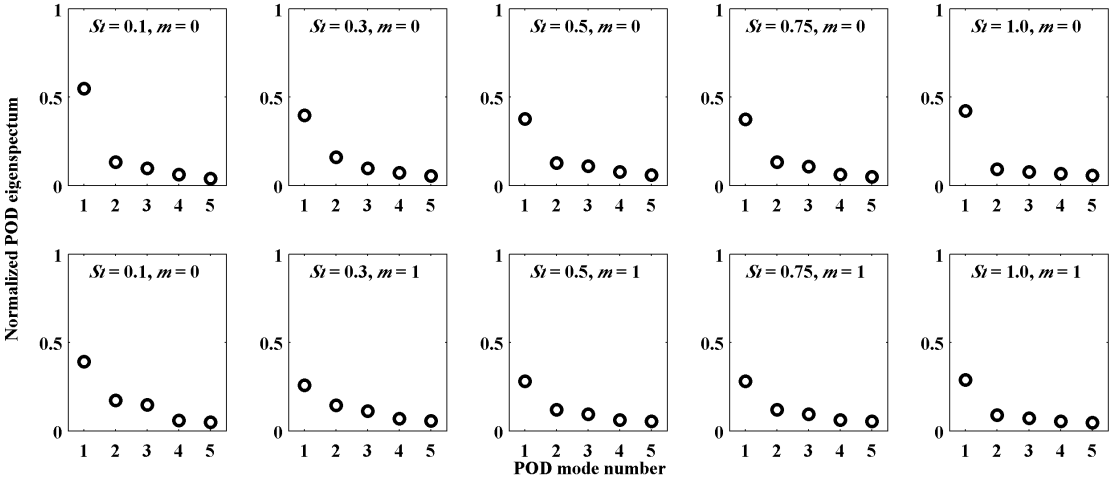

Figure 1. Normalized spectra of POD eigenvalues $\sigma^j / \sum_l \sigma^l$ for the B118 jet at several Fourier modes.

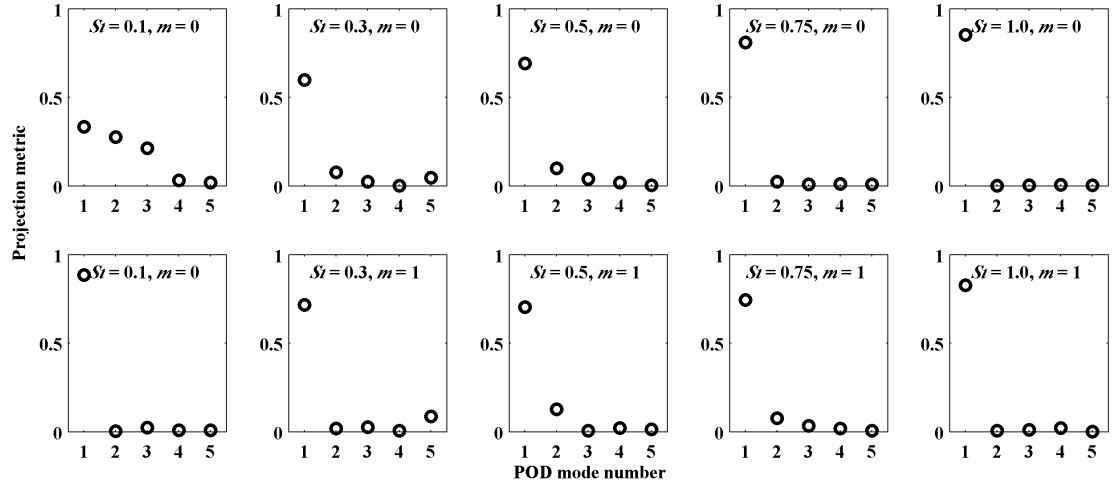

Figure 2. Projection metric Λ^j represented by the PSE solution, as projected on to the corresponding POD modes, for the B118 jet at several Fourier modes.

This section compares the PSE solutions with POD modes extracted from the LES database. For brevity, the presentation of results will consider the frequencies $St = \{0.1, 0.3, 0.5, 0.75, 1\}$ and $m = 0$ and $m = 1$ azimuthal modes, which cover the range of large-scale structures most significant for the aft peak noise radiation. Comparisons at higher frequencies are not done here; the far-field spectra shows that the noise radiated at $St = 1$ is already an order of magnitude lower that the peak.[31]

The POD yields an orthogonal basis set, so that the PSE solution can be orthogonally projected onto the individual POD using the inner product given in (9). The magnitude of the projection coefficient is a

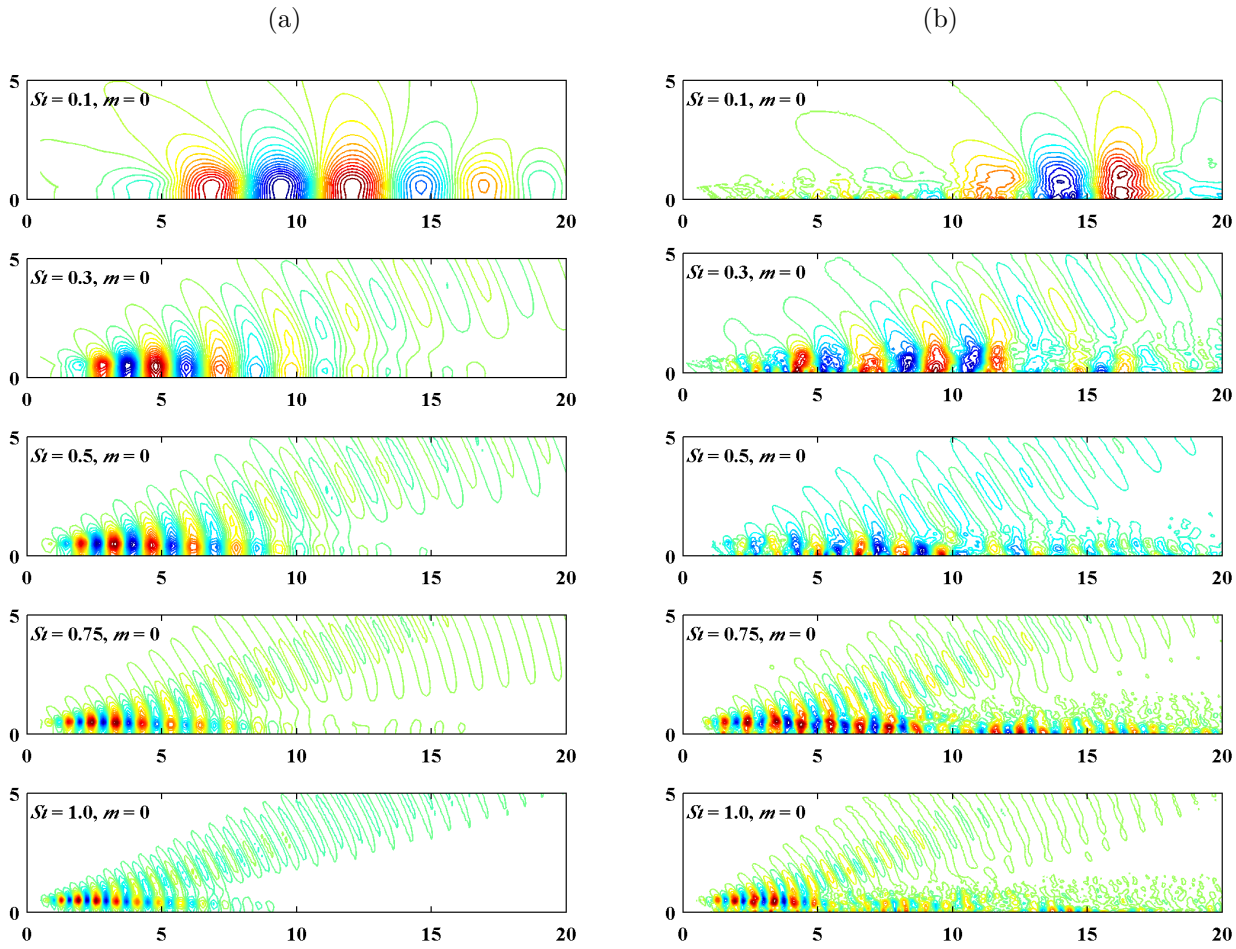

Figure 3. Comparison of the pressure component of (a) PSE solution with (b) corresponding first POD modes with $m = 0$, for the B118 case.

measure of the correlation of the PSE solution and the corresponding POD mode:

$$\Lambda^j = \frac{< \breve{\mathbf{q}}(x,r), \breve{\phi}^j(x,r) >}{\|\breve{\mathbf{q}}(x,r)\| \; \|\breve{\phi}^j(x,r)\|}. \tag{12}$$

A value of the metric Λ^j close to 1 for the first POD mode indicates that the PSE solution is representative of the most coherent wavepacket found in the flow.

Figure 1 shows the POD eigenvalues for some representative Fourier modes, for the cold B118 jet. While the first eigenvalue attains values close to 0.5 for most of the Fourier modes depicted, the decay rate of the spectra is relatively low. The flatness of the spectra means that many mutually orthogonal modes are dynamically significant; it increases at higher frequencies and azimuthal mode numbers. It is well recognized in the literature[21] that the flatness of the POD spectra increases with the size of the domain owing to the relation of POD modes with Fourier modes and the finite integral lengths of the flow. Rapid variations in wavepacket's amplitude or phase speed in time and space would require more POD modes in the reconstruction.

Figure 2 compares the pressure component of the PSE solution with the corresponding first POD modes using the metric Λ^j introduced above. Apart from the $St = 0.1, m = 0$ Fourier mode, to be discussed later, all other PSE modes demonstrate very good matches with the most coherent structures present in the data. Visual comparisons of the PSE solutions with the first POD modes for the Fourier modes under consideration are depicted in figures 3 and 4. Only the real parts of the pressure component are shown. Both the linear PSE modes and the POD modes have arbitrary amplitude and phase, so that only their

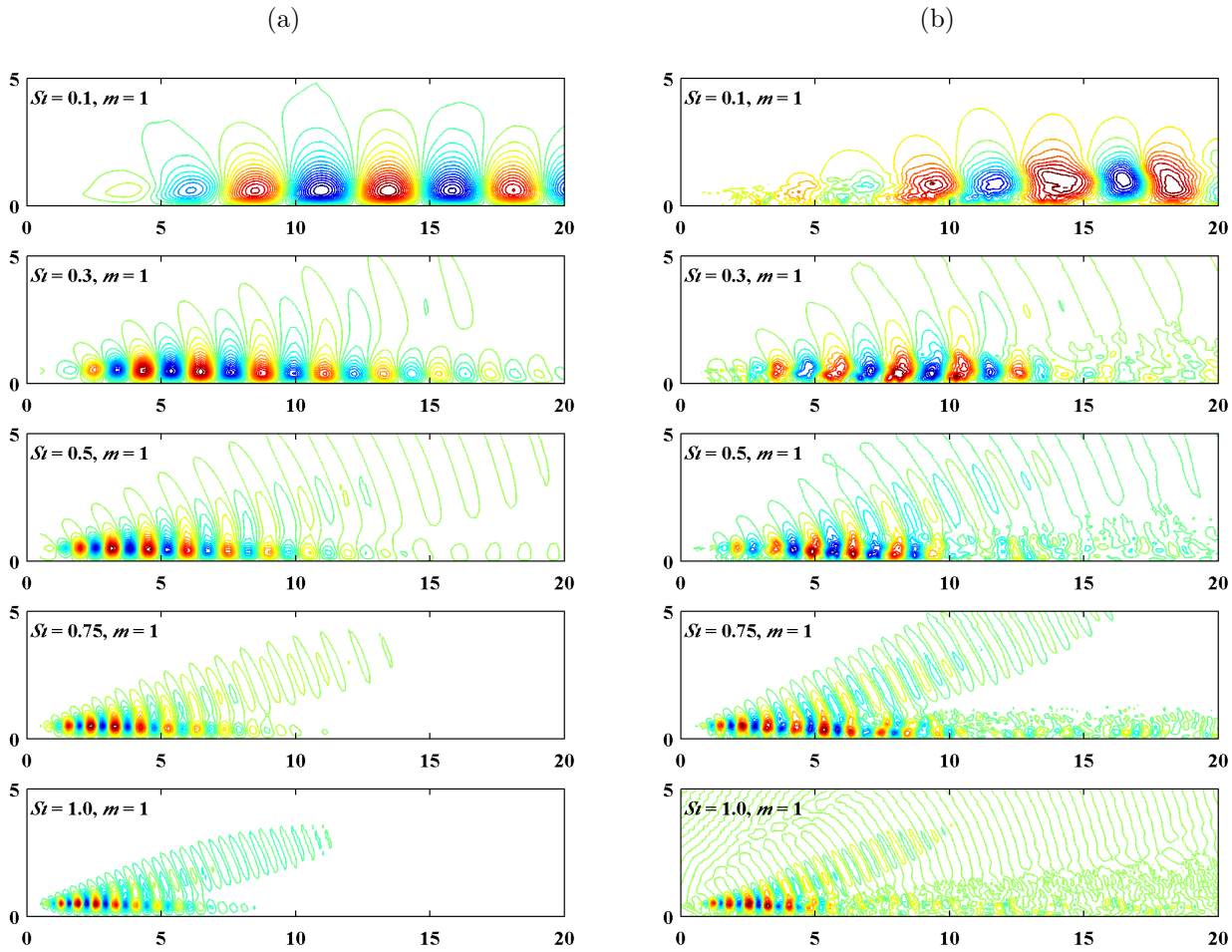

Figure 4. Comparison of the pressure component of (a) PSE solution with (b) corresponding first POD modes with $m = 1$, for the B118 case.

spatial structures (i.e. the relative amplitudes and phases) are pertinent in the figures. Significant similarity is observed for all the Fourier modes except the first one, explaining the metric values shown in figure 2. For the higher frequencies considered herein ($St = 0.3$ and 0.5), both the PSE solutions and POD modes exhibit clear, highly directional radiation patterns. These patterns are most relevant for modeling the far-field noise and are shown to be captured quite well by the PSE. Such radiation patterns are not readily observed for the $St = 0.1$ modes, probably due to the low radiating efficiency at these frequencies. In a previous work considering the same jet configurations,[33] the computed PSE solutions did not contained the radiation pattern. As discussed earlier, a spatial filter was applied to the mean flow in that work, that was found to be too aggressive. In the present work the time-averaged mean flow is employed unfiltered.

The case of the $St = 0.1, m = 0$ Fourier mode is investigated further in figure 5. It was observed in figure 2 that the first 3 POD modes all have a similar but moderate correlation with the PSE solution. Figure 5 reveals that the PSE solution has nearly uniform amplitude over a large part of the streamwise domain, but none of the POD modes are as such. As opposed to the other Fourier modes, for $St = 0.1, m = 0$ none of the first 3 POD modes exhibit a clear wave structure over a significant spatial region, whereas the PSE Ansatz imposes the wave-like behavior. Modeling low-frequency modes with PSE has proven challenging for subsonic[13,23] and supersonic[33,37] jets previously. A possible cause of this discrepancy is that the assumption of slow streamwise variation of the base flow (compared to the wavepacket wavelength) becomes tenuous at this low frequency. One the other hand, possible nonlinear interactions between the resolved Fourier modes, that are neglected in the present work, tend to have a stronger effect on the evolution of the lower (in frequency and azimuthal wavenumber) Fourier modes.[40]

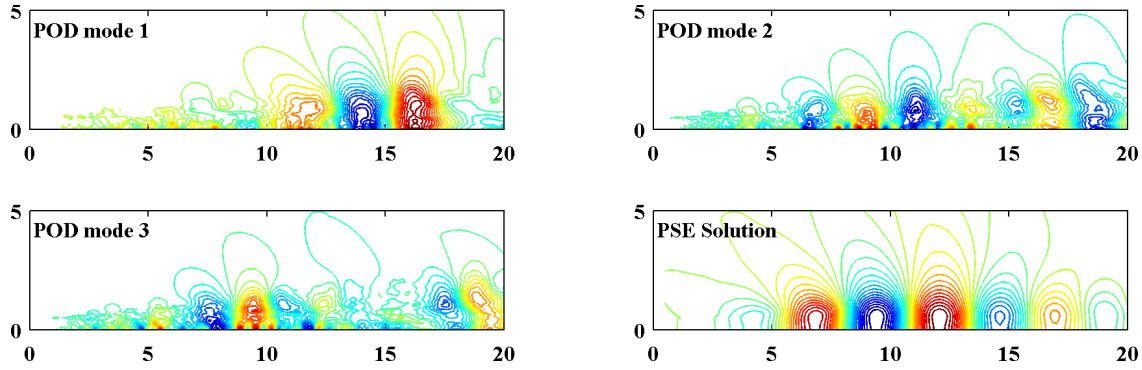

Figure 5. Comparison of the first 3 pressure POD modes of the $St = 0.1, m = 0$ Fourier modes with the corresponding PSE solution for the B118 case. The color-scales of the POD modes reflect their relative energies in the eigenspectrum.

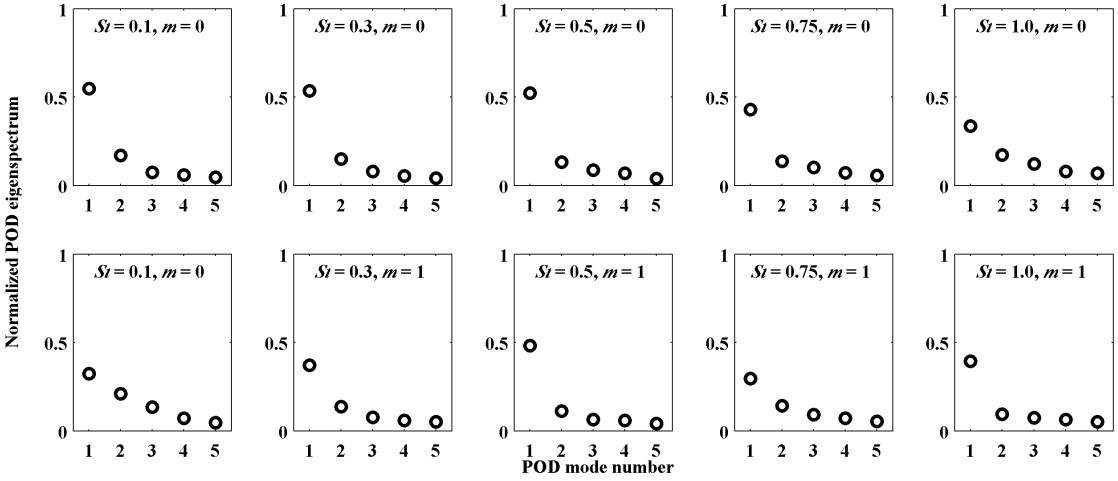

Figure 6. Normalized spectra of POD eigenvalues $\sigma^j / \sum_l \sigma^l$ for the B122 jet at several Fourier modes.

Attention is now turned to the heated B122 supersonic jet; the presentation of the results follows the preceding scheme. The POD eigenvalues, shown in figure 6, follow the same trends discussed for the cold B118 jet. There is no dramatic change in the degree of coherence when the jet is heated, but here the significance of the first POD mode is even higher than for the cold jet, as the leading POD eigenvalue exceeds 0.5 in most cases. Figure 7 shows that the projection of the PSE solution represented by the first POD modes also follows the trends found in the B118 case. However, significant discrepancies are exhibited by the $St = 0.3, m = 0$ Fourier mode now, in addition to the $St = 0.1, m = 0$ mode.

Figures 8 and 9 presents visual comparisons of the PSE solutions with the first POD modes as before. The overall match between the two appear quite acceptable. In particular, the linear PSE appears to correctly capture the increased polar angle of the peak radiation caused by the increased jet velocity. Regarding the $St = 0.3, m = 0$ Fourier mode, the LES indicates a peak near the end of the potential core (around $x = 7$) which the PSE fails to replicate. This possibly implicates nonlinear effects at the merger of the shear layer at this frequency too.

V. Acoustic far-field of wavepackets

The propagation to the far-field of the pressure field corresponding to the PSE wavepacket models is presented in this section, along with comparisons against the acoustic data from the LES database.

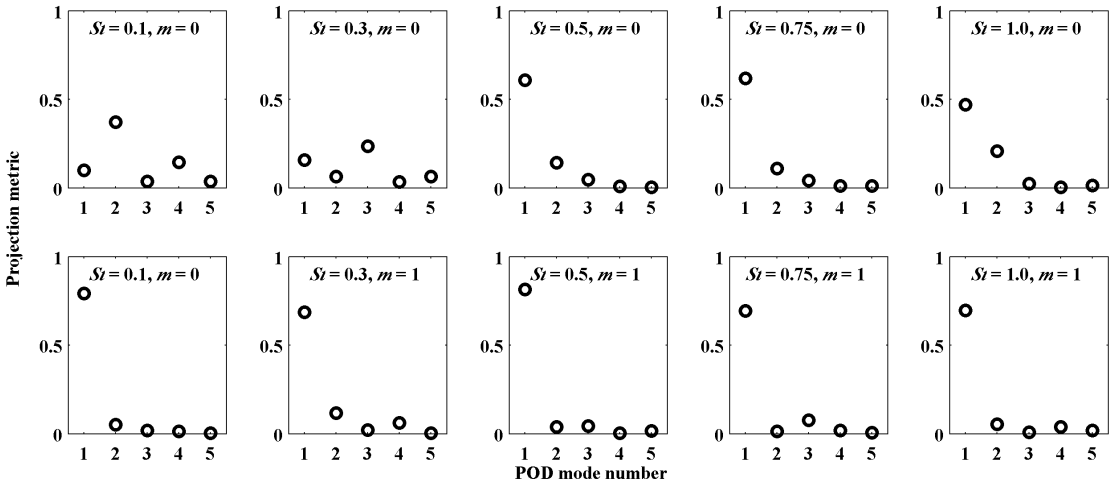

Figure 7. Projection metric Λ^j represented by the PSE solution, as projected on to the corresponding POD modes, for the B122 jet at several Fourier modes.

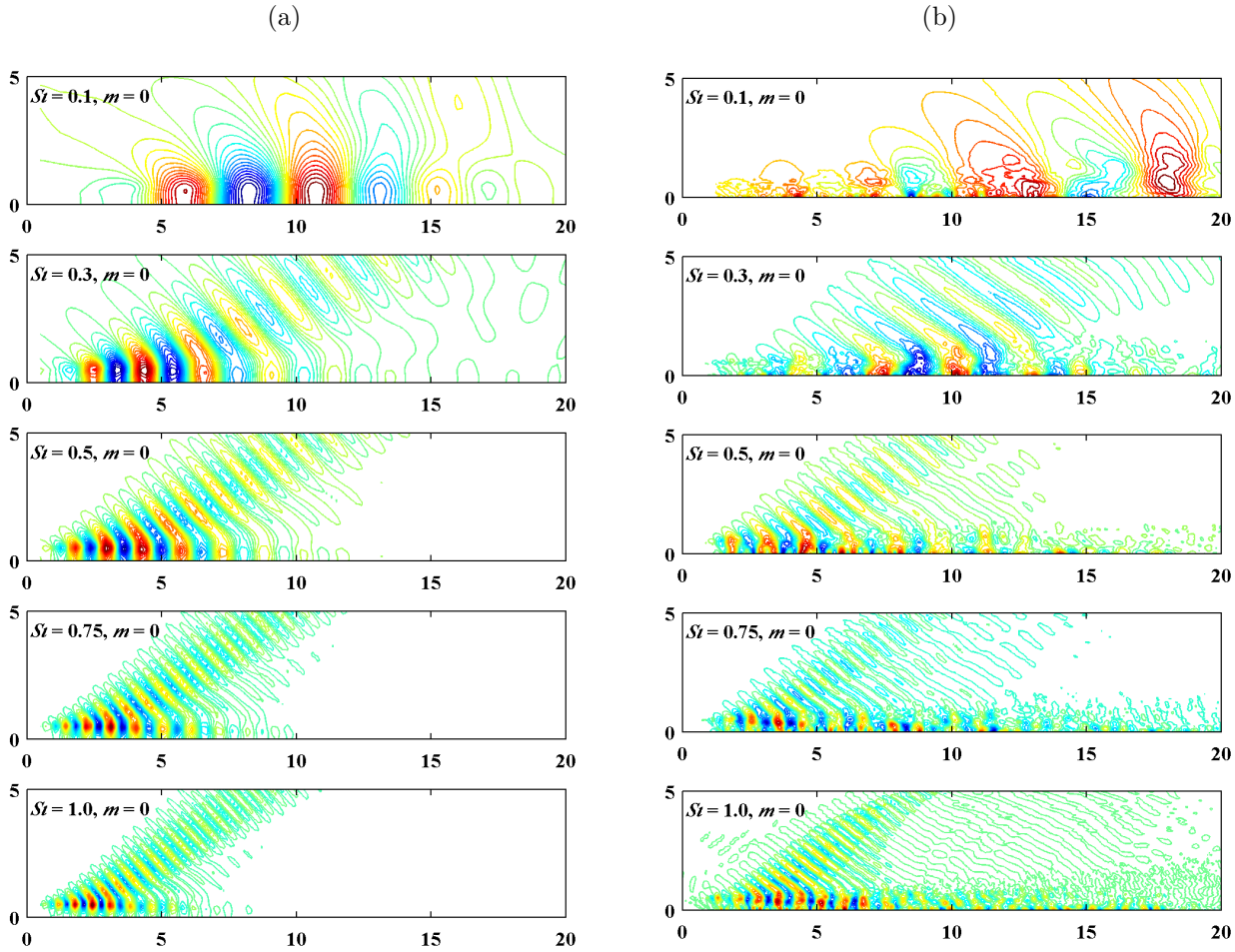

Figure 8. Comparison of the pressure component of (a) PSE solution with (b) corresponding first POD modes with $m = 0$, for the B122 case.

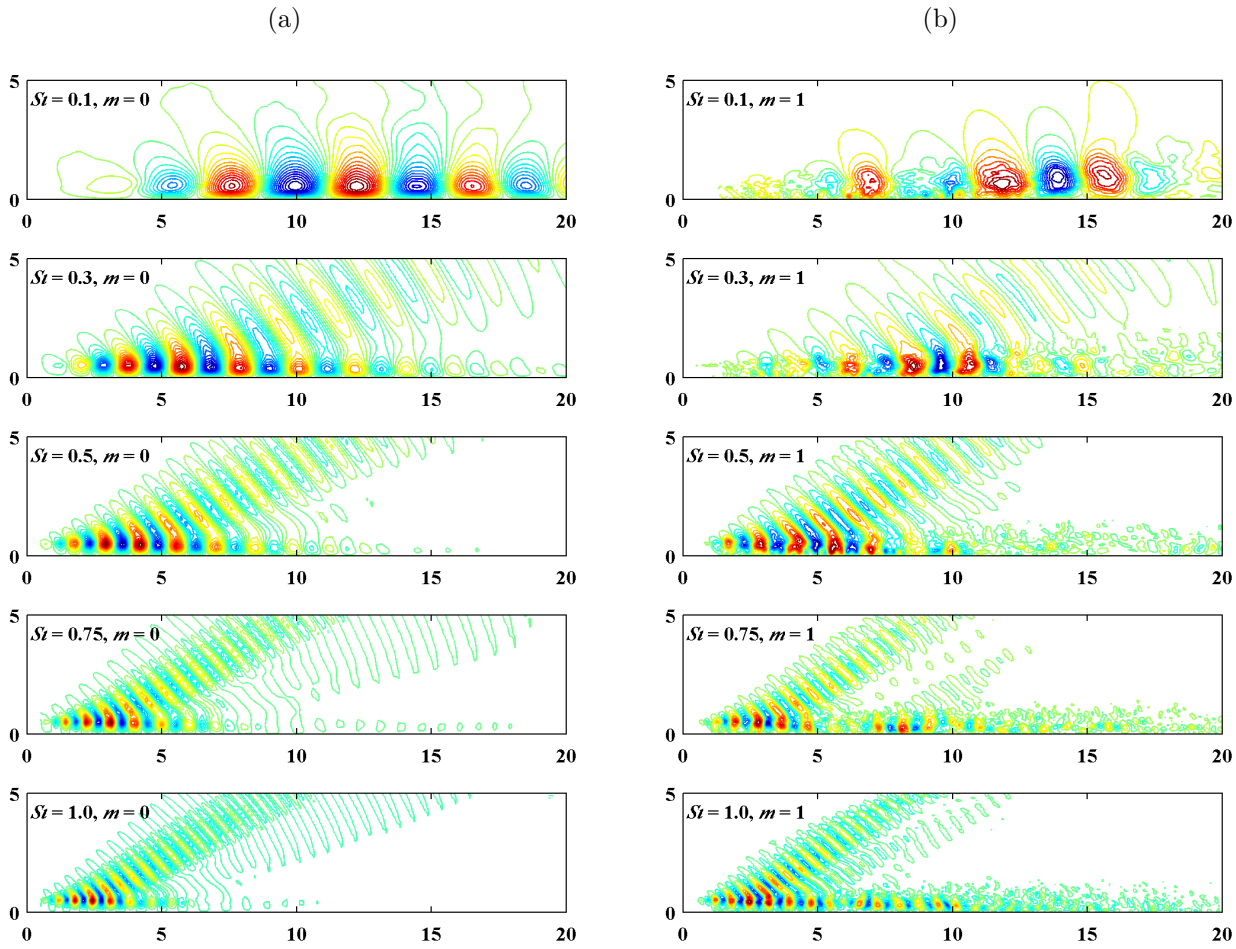

Figure 9. Comparison of the pressure component of (a) PSE solution with (b) corresponding first POD modes with $m = 1$, for the B122 case.

A. Formulation of the Kirchhoff surface method

Following Lighthill's theory,[24] in those cases in which the processes involved in noise generation have a compact support and the generation and propagation of noise can be separated as independent phenomena, the acoustic pressure propagated on an uniform stream can be computed as the solution of the forced wave equation

$$\frac{\partial^2 p}{\partial t^2} + 2\bar{u}_{co}\frac{\partial^2 p}{\partial x \partial t} + \bar{u}_{co}^2\frac{\partial^2 p}{\partial x^2} - \nabla^2\ p = S, \tag{13}$$

where the forcing term S accounts for the noise sources and takes the form

$$S = \nabla \cdot \nabla \cdot (\rho \mathbf{v} \cdot \mathbf{v} - \tau) + \left(\frac{\partial^2}{\partial t^2} + 2\bar{u}_{co}\frac{\partial^2}{\partial x \partial t} + \bar{u}_{co}^2\frac{\partial^2}{\partial x^2}\right)(p - \rho). \tag{14}$$

Here τ denotes the viscous part of the stress tensor. Its contribution is usually neglected due to the high Reynolds number and original arguments from Lighthill,[24] and was shown to have a negligible effect even at Reynolds numbers as low as 200.[41] The term $\bar{u}_{co}$ stands for an uniform co-flow component, usually existing in jet experiments.

A decomposition of the flow variables into time-averaged mean flow and fluctuations is introduced now, in line with the PSE decomposition. Fourier modes in time and azimuthal direction are also introduced, leading to

$$\left[(1-\bar{u}_{co}^2)\frac{\partial^2}{\partial x^2}+2\mathrm{i}\omega\bar{u}_{co}\frac{\partial}{\partial x}+\frac{1}{r}\frac{\partial}{\partial r}\left(r\frac{\partial}{\partial r}\right)-\frac{m^2}{r^2}+\omega^2\right]\ \breve{p}(x,r;\omega,m)=\breve{S}(x,r;\omega,m). \tag{15}$$

The source term (14) is linearized about the mean flow and non-linear interactions are neglected. These non-linear terms, responsible for the *self-noise* production have been pointed out as the main noise source at side-line angles,[42] and as one possible mean of nonlinearity on the noise propagation.[11] Here, these terms are neglected in the aim of computing the acoustic field associated with the single-frequency wavepacket, and are assumed to have a relatively small importance in the noise emitted at low angles.

Equation (15) is a two-dimensional inhomogeneous Helmholtz equation, that governs the propagation of pressure waves. Following the principle of causality, waves must propagate from the compact-supported source outwards, verifying Sommerfeld's radiation condition. At the axis, the solution has to be bounded for axisymmetric modes and vanish for $m \neq 0$.[43] The solution of this problem by means of the Green's function technique is an standard procedure that is very efficient when the solution is only required for a small number of points, e.g. on an arc at a large distance from the nozzle. On the other hand, if the solution on a (x,r)-plane is sought for, the convolutions required for a two-dimensional space make the computation prohibitive. A different approach is followed here. A Fourier transform is applied along the axial direction, using the transformation pair

$$\tilde{p}(r;k,\omega,m)=\int_{-\infty}^{\infty}\breve{p}(x,r;\omega,m)\ \mathrm{e}^{-\mathrm{i}kx}dx,\quad \breve{p}(x,r;\omega,m)=\frac{1}{2\pi}\int_{-\infty}^{\infty}\tilde{p}(r;k,\omega,m)\ \mathrm{e}^{\mathrm{i}kx}dk, \tag{16}$$

and resulting into the one-dimensional Helmholtz equation

$$\left[\frac{1}{r}\frac{\partial}{\partial r}\left(r\frac{\partial}{\partial r}\right)-\frac{m^2}{r^2}+\lambda^2\right]\ \tilde{p}(r;k,\omega,m)=\tilde{S}(r;k,\omega,m)=\int_{-\infty}^{\infty}\breve{S}(x,r;\omega,m)\ \mathrm{e}^{-\mathrm{i}kx}\ dx. \tag{17}$$

The real axial wavenumber is denoted by k in order to avoid confusions with the complex wavenumber α used in PSE. The variable $\lambda^2=\omega^2-k^2(1-\bar{u}_{co}^2)-2k\omega\bar{u}_{co}$ has been introduced. A general solution to (17) can be obtained by using the Green's function technique.[43] However, the noise source in turbulent jets is compact in the radial direction and decays several orders of magnitude in a short distance from the lipline.[8,10,44] Thus, if the pressure is known on a surface bounding the source, equation (17) reduces to an homogeneous boundary value problem. A particularly simple solution[1] exists if the boundary surface is a cylindrical Kirchhoff surface of radius r_0. Then, for any radius $r > r_0$:

$$\tilde{p}(r;k,\omega,m)=\tilde{p}(r_0;k,\omega,m)H_m(\lambda r)/H_m(\lambda r_0), \tag{18}$$

where it was assumed that $\omega > 0$ and H_m is Hankel function of the first kind. Note that the value of λ is determined by the corresponding value of k, for fixed values of the other parameters. λ is double-valued for each k. By analyzing the asymptotic behavior of the Hankel function as $r \to \infty$, while noting the $e^{-\mathrm{i}\omega t}$ criteria followed for the temporal Fourier transform, it can be shown that for $r > 0, \omega > 0$, the negative branches (real or imaginary) of λ are not valid solutions of the present problem, and only the positive branches are taken into account in the numerical solution of the problem. Finally, by application of the inverse Fourier transform in the axial direction, the acoustic field $p(x,r;\omega,m)$ is obtained.

The validation of the acoustic field computation using equation (18) is performed here using the LES databases for the isothermal and heated supersonic jets. The domain on which data is available is $0 \leq x \leq 20$, $0 \leq r \leq 5$. The cylindrical surface is placed at $r_0 = 3$, and the resultant pressure signal at $r_0 = 4.5$ is computed for one segment of data of length $40D^*/U_j^*$. The co-flow $\bar{u}_{co} = 0.1$ was considered in arriving at this prediction. Comparison with the direct data from LES in figure 10 validates the technique. Note that an exact match is not expected since both the source and destination surfaces are probed over the same time window (of duration $20D^*/U_j^*$) for computing the Fourier transforms, which ignores the effect of propagation delay ($\approx 2.25D^*/U_j^*$).

B. Amplitude calibration of the PSE solutions

The governing equations (4) are linear; consequently the computed solutions are arbitrary with respect to a complex factor, accounting for the amplitude. Ideally, the missing scale factor would be determined from knowledge of the inlet perturbations in empirical data, i.e. data from experiments or numerical simulations,

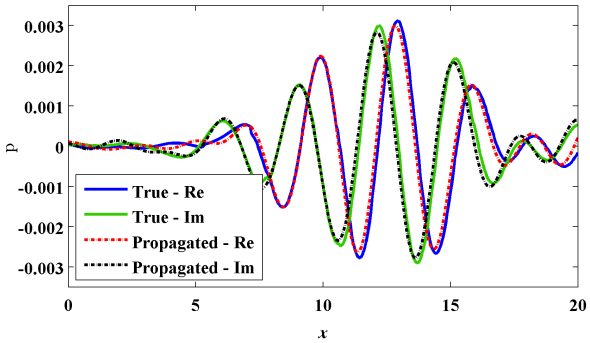

Figure 10. Pressure signature predicted at $r = 4.5$ from the data available at $r = 3$ for $St = 0.3, m = 0$, compared with the true value from the B118 LES data.

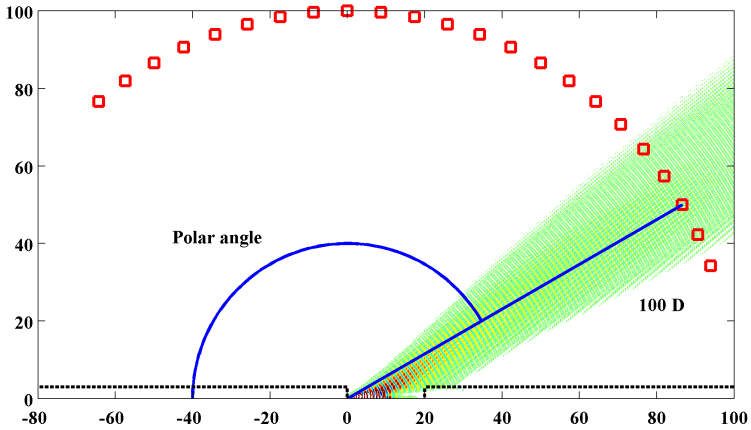

Figure 11. Extension of PSE wavepacket to the acoustic far field, $St = 0.3, m = 0$, illustrating the location of the far-field arc (red squares).

that are usually known on a stochastic basis. In order to compare to averaged data from experiments or simulations, the scaling factors would then be averaged, with no changes in the shape of the PSE solution.

Different possibilities were explored in the past for the determination of the wavepacket amplitudes. Tam and Chen[45] proposed a method for the determination of the stochastic wave packet amplitudes, by assuming that the K-H instability wave was representative of all the fluctuation energy content at each frequency and matching it to the turbulent kinetic energy at the nozzle lip. Another possibility is to determine the scale factor in order to obtain the best agreement with wavepacket signatures measured empirically, either in the pressure near-field,[13] in the velocity field[13, 23, 46] or in the acoustic far field.[8] In the present research, the availability of high-fidelity LES data enables us to explore different possibilities.

In the preceding sections the PSE solutions were shown to be in good agreement with the first POD modes of the LES database, suggesting the scaling of the PSE solution to best fit the amplitude of the leading POD mode. Instead of using the full domain of the computed POD modes in the fitting, the pressure components at two different surfaces are employed. This is done in the aim of showing the consistency of the PSE solutions over the near field. In the first case the amplitude is fitted with the POD pressure at the Kirchhoff surface cylinder ($r_0 = 3$) using a least mean squares method. In the second case the amplitude fitting is done at a conical surface mimicking the near-field microphone cage that was used in the experiments performed at UTRC,[30] similarly to our previous research on subsonic jets.[13, 29] The cage cone has a half-angle of 7° to the jet axis, and intercepts the nozzle exit cross-section at $r = 0.88$.

Another method of calibrating the PSE solutions is possible thanks to the LES database. Instead of using empirical data along the axial direction, the fluctuations at a near-nozzle cross-section are extracted from the LES database and used to determine the inlet PSE amplitude $A_{\omega m}(x_0)$ for each Fourier mode.[37] The bi-orthogonality between the eigenfunctions of (6) and those corresponding to its adjoint is exploited to determine the inlet amplitudes

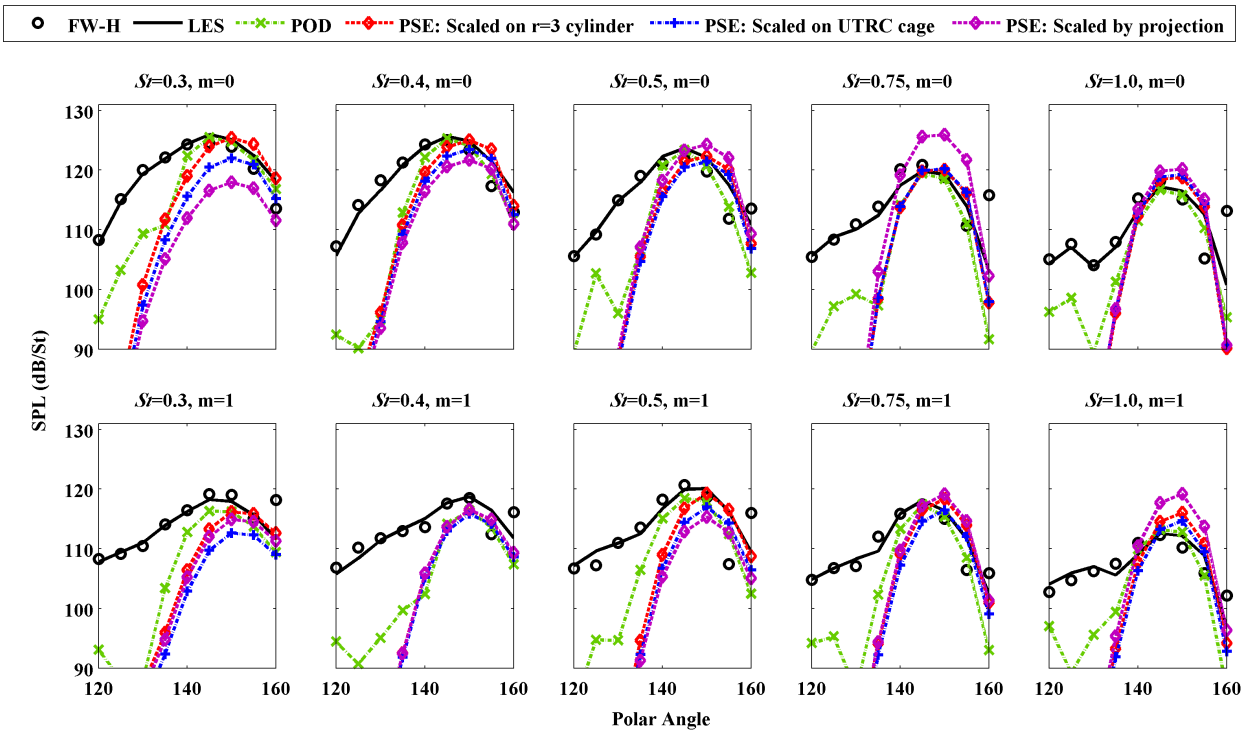

Figure 12. Far field acoustic predictions at 100 diameters for B118 jet, comparing results from the projection of linear PSE, POD and the full LES fluctuation information on the $r_0 = 3$ surface, and the FW-H method.[31]

$$A_{\omega m}(x_0) = \left(\left(\hat{\mathbf{q}}^{+}_{\omega m} \right)^H \mathbf{L}\, \breve{\mathbf{q}}_{LES}(x_0) \right) / \left(\left(\hat{\mathbf{q}}^{+}_{\omega m} \right)^H \mathbf{L}\, \hat{\mathbf{q}}_{\omega m} \right). \tag{19}$$

In (19), $\hat{\mathbf{q}}_{\omega m}$ and $\hat{\mathbf{q}}^{+}_{\omega m}$ are the direct and adjoint eigenfunctions corresponding to the K-H eigenmode, and $\breve{\mathbf{q}}_{LES}$ is the Fourier-transformed fluctuation profile at $x_0 = 0.5$ extracted from the LES database. As was done in the computation of the POD modes, short-time Fourier transform is performed using respectively 29 and 19 data segments for the B118 and B122 jets. For each segment, the Fourier-transformed segment is projected on the K-H eigenmode determining the amplitude for the PSE solution. The projection amplitudes are then averaged over segments. It should be remarked that the bi-orthogonal projection method is more stringent than fitting to the POD modes, as information at a single cross-section is used to determine the wavepacket amplitudes, without further knowledge of the fluctuations along the streamwise direction.

C. Far-field results and comparison with projected LES data

Figure 11 shows the projected acoustic field for mode $St = 0.3$ and $m = 0$. The cylindrical surface is placed at $r_0 = 3$ and extends over $0 \leq x \leq 20$. Directivity plots are considered in what follows to perform the comparisons. Instead of probing the pressure field at the same locations as in UTRC experiments,[30,31] the far-field pressure at a circular arc located at a distance of 100 diameters from the nozzle exit is considered in the present work.

Comparisons are done with results of the Ffowcs Williams-Hawkings (FW-H) solution of Brès *et al.*,[31] that does not consider the co-flow when propagating to the far-field. Their FW-H solution, in turn, was validated with experimental data acquired at the UTRC facility which has a co-flow $\bar{u}_{co} = 0.1$ created with a duct of diameter 10 diameters. The shear-layer between the co-flow and the ambient is difficult to account for in the sound propagation calculations, and was hence avoided altogether. Consequently, the effect of the co-flow will also be neglected in the present far-field computations. In order to illustrate the similarity between the FW-H solution, and the present Kirchhoff surface method, the far field is computed applying the latter to the Fourier-decomposed LES fluctuations at $r_0 = 3$. Comparisons are shown in figures 12 and

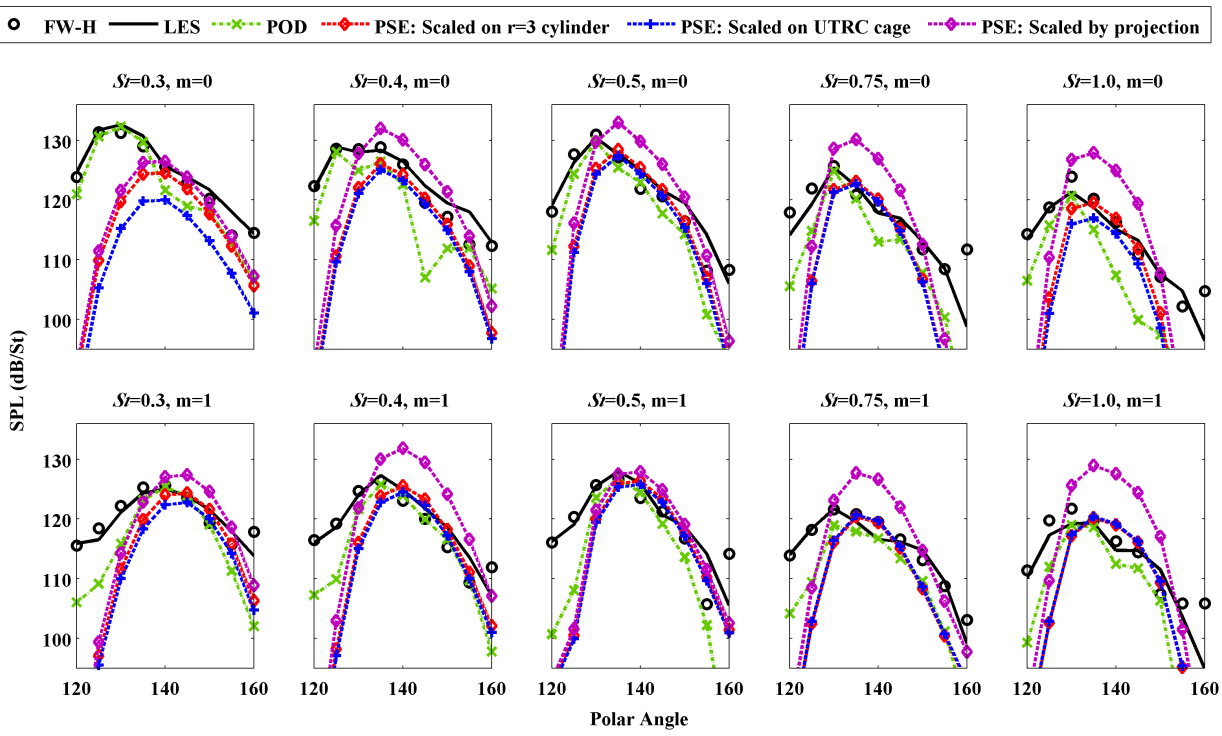

Figure 13. Far field acoustic predictions at 100 diameters for B122 jet, comparing results from the projection of linear PSE, POD and the full LES fluctuation information on the $r_0 = 3$ surface, and the FW-H method.[31]

13 (black symbols and lines), showing a very good agreement. The discrepancies observed at low frequencies and angles close to the jet axis are attributed to the differences between the FW-H and the present Kirchhoff surface methods: the former employed end-caps to account for the acoustic source flux at the downstream end of the domain, while this effect is ignored in the present method. Consequently, the discrepancies are most prominent at low frequencies and higher polar angles. In what follows, comparisons are restricted to $St \geq 0.3$ and polar angles $\leq 160°$.

Figure 12 shows the far-field directivity plots computed for the B118 jet for some (St, m) Fourier modes. In addition to the acoustic field corresponding to the projected LES data, four predictions are shown: the acoustic projection of the first POD eigenmode and PSE solutions scaled in the three different ways described in section V.B. The directivity plots corresponding to the POD mode and PSE solution are nearly identical near the intensity peak (polar angle $\approx 150°$), where they also match the directivity shapes corresponding to the projection of the the projection of the unfiltered LES data reasonably well. With respect to the amplitudes, the POD mode recovers the peak amplitude of the unfiltered LES data. The PSE solutions fitted using the POD data differ by less than $1 - 2$dB for the frequencies analyzed, except for the lowest $St = 0.3$. The calibration using the bi-orthogonal projection also delivers good overall comparisons, with incidental under-predictions $(St = 0.3, m = 0)$ or over-predictions $(St = 0.75, m = 0)$.

Figure 13 shows the analogous directivity plots for the heated B122 jet. For this jet configuration, the peak occurs at lower $(140° - 145°)$ polar angles with the jet axis due to the increase in the acoustic jet Mach number. The comparisons both in shape and amplitude are again good, with deviations of few dBs in the near peak region. A general tendency is observed in the results calibrated by bi-orthogonal projection to over-predict the amplitudes, that was not clearly observable for the B118 jet.

VI. Conclusions

PSE have been proposed as a tool for developing reduced-order models of the wavepackets implicated in peak sound radiation to the far field for turbulent jets. Previously, we have shown that linear PSE is

indeed effective in predicting the near-field hydrodynamic pressure signature of wavepackets in turbulent subsonic jets. Results presented here indicate reasonable match between PSE predictions and observations of the streamwise evolution of acoustically-important wavepackets both in the near and far acoustic fields of supersonic jets. The present investigation considered two ideally-expanded jets, one isothermal and one moderately heated, for which a high-quality LES database was available. Special care was taken in the set up of the simulations in order to have a very long time sample to achieve reasonable statistical convergence of the low frequencies, and a fine spatial resolution in the vicinity of the nozzle lip to reproduce accurately the initial shear layer. The availability of the detailed flow information in the LES database has been crucial for developing and validation of the models.

The proposed linear wavepacket models require two inputs that are provided by the LES database: the mean flow field, and information to determine the amplitude of the wavepackets. The mean flow enters into the PSE model nonlinearly and incorporates the major coupling effects of all scales in the flow. It is only when the wavepackets are considered as stochastic objects residing on top of the mean flow that it can be concluded that their dynamics are predominantly linear. The wavepacket models have been validated against the LES database. One of the difficulties in evaluating the models is the extraction of the relevant noise-radiating large-scale flow structures from empirical data of unforced jets, due to their relatively low energy. Following previous experiences in subsonic jets,[13,23,33] POD was used here in order to filter out the uncorrelated fluctuations. The availability of data on a relatively fine mesh enables us to compute planar (x, r) POD modes corresponding to the (St, m) Fourier modes, that are compared directly with the pressure component of PSE solutions. The comparison with POD-filtered data is more challenging than in the subsonic jets, due to the increased intensity of the acoustic field with the jet Mach number, that becomes comparable to the large-scale hydrodynamic fluctuations. However, careful analysis of the POD results presented herein reveals acceptable fidelity of the PSE model. A very good agreement is found between the PSE solution and the first POD mode for most of the frequencies of interest. At the lower end of the acoustically important range ($St \approx 0.1$), a poor match is persistently being observed in the near-field structure of the pressure field, in line with the findings in subsonic jets. A possible cause for this discrepancy is related to the assumption of slowly-diverging mean flow, as for low frequencies the wavepacket wavelength becomes comparable to the length of the potential core. The PSE Ansatz should be then relaxed and a global eigenmode analysis would be pertinent.[47] Another possibility is that the nonlinear interactions between the resolved Fourier modes, neglected in the present linear PSE computations, are significant in the evolution of the lower Fourier modes.[40]

The solutions of linear PSE are arbitrary with respect to the amplitude. Fluctuation data from LES can be used in different manners in order to determine the wavepacket amplitudes; one of the possibilities considered here performs a least mean-squares fitting of the PSE pressure amplitude to the most coherent structures extracting using full-domain POD, at selected surfaces in the near acoustic field. The consistency of the near pressure field of PSE computations and POD modes results in very similar wavepacket amplitudes when the amplitude fitting is performed at different surfaces. Another possibility investigated here makes use of the bi-orthogonality relation between the direct and adjoint eigenfunctions of the parallel-flow linear stability problem, in order to project the LES data at a single near-nozzle cross-section on the Kelvin-Helmholtz eigenmode. In this manner, the amplitude of the PSE model is determined without knowledge of the fluctuations' evolution over the streamwise domain. Finally, the amplitude-scaled wavepackets are extended to the acoustic far field by imposing the pressure distribution from the PSE solution extracted at a circular cylinder in the near field as an inhomogeneous boundary condition in the solution of the Helmholtz equation. The extended wavepackets compare reasonably well with the far-field pressure from the LES database, especially near the directivity peak.

In sum, the present paper demonstrates, by means of quantitative comparisons with LES data, that linear instability waves computed by PSE are a valid model for the wavepackets existing in supersonic turbulent jets. The modeled near field is shown to correlate strongly with the most coherent structures in the flow, identified as the leading POD modes. In addition, after fitting the PSE model amplitude in the near field, the direct projection to the far field reproduces robustly the peak noise directivity and magnitude.

Acknowledgements

This work was sponsored in part by the U.S. Navy Naval Air Systems Command (Contract N68335-11-C-0026) and by the Office of Naval Research (Grant N0014-11-1-0753). Any opinions, findings, and conclusions or recommendations expressed in this material are those of the author(s) and do not necessarily reflect the views of the sponsoring agencies. The LES calculations were carried out on CRAY XE6 machines at DoD supercomputer facilities in ERDC and AFRL. D. Rodríguez acknowledges funding from the Marie Curie - COFUND-UNITE programme.

References

[1]C. Tam, D. Burton, Sound generated by instability waves of supersonic flows. Part 2. Axisymmetric jets., J. Fluid Mech. 138 (1984) 273–295.

[2]E. Mollo-Christensen, Jet noise and shear flow instability seen from an experimenter's viewpoint, J. Applied Mech. 34 (1967) 1–7.

[3]G. L. Brown, A. Roshko, On density effects and large structure in turbulent mixing layers, J. Fluid Mech. 64 (1974) 775–816.

[4]A. Michalke, H. V. Fuchs, On turbulence and noise of an axisymmetric shear flow, J. Fluid Mech. 70 (1975) 179–205.

[5]P. Jordan, T. Colonius, Wave Packets and Turbulent Jet Noise, Annu. Rev. Fluid Mech. 45 (1) (2013) 173–195.

[6]D. G. Crighton, M. Gaster, Stability of slowly diverging jet flow, J. Fluid Mech. 77 (2) (1976) 397–413.

[7]F. P. Bertolotti, T. Herbert, P. Spalart, Linear and nonlinear stability of the blasius boundary layer, J. Fluid Mech. 242 (1992) 441–474.

[8]P. Balakumar, Prediction of supersonic jet noise, AIAA Paper 1998-1057.

[9]C. C. Yen, N. L. Messersmith, Application of parabolized stability equations to the prediction of jet instabilities, AIAA J. 36 (1998) 1541–1544.

[10]E. Piot, G. Casalis, F. Muller, C. Bailly, Investigation of the pse approach for subsonic and supersonic hot jets. detailed comparisons with les and linearized euler equations results, Int. J. Aeroacoustics 5 (2006) 361–393.

[11]N. Sandham, A. Salgado, Nonlinear interaction model of subsonic jet noise, Phil. Trans. Roy. Soc. A 366 (2008) 2745–2760.

[12]L. Cheung, S. Lele, Linear and nonlinear processes in two-dimensional mixing layer dynamics and sound radiation, J. Fluid Mech. 625 (2009) 321–351.

[13]K. Gudmundsson, T. Colonius, Instability wave models for the near-field fluctuations of turbulent jets, J. Fluid Mech. 689 (2011) 97–128.

[14]M. R. Malik, C. L. Chang, Nonparallel and nonlinear stability of supersonic jet flow, Computers and Fluids 29 (2000) 327–365.

[15]R. Mankbadi, J. T. C. Liu, A study of the interactions between large-scale coherent structures and fine-grained turbulence in a round jet, Proc. Roy. Soc. London 1443 (1981) 541–602.

[16]P. Ray, L. Cheung, S. Lele, On the growth and propagation of linear instability waves in compressible turbulent jets, Physics of Fluids 21 (2009) 054106.

[17]J. T. C. Liu, Developing large-scale wavelike eddies and the near jet noise field, J. Fluid Mech. 62 (1974) 437–464.

[18]P. Morris, M. Giridharan, G. Lilley, On the turbulent mixing of compressible free shear layers, Proc. R. Soc. Lond. A. 431 (1990) 219–243.

[19]C. Tam, P. Morris, Tone excited jets – Part V: A theoretical model and comparison with experiments, J. Sound Vib. 102 (1985) 119–151.

[20]T. Suzuki, T. Colonius, Instability waves in a subsonic round jet detected using a near-field phased microphone array, J. Fluid Mech. 565 (2006) 197–226.

[21]P. Holmes, J. Lumley, G. Berkooz, Turbulence, Coherent structures, dynamical systems and symmetry, Cambridge University Press, New York, 1996.

[22]R. E. A. Arndt, D. Long, M. Glauser, The proper orthogonal decomposition of pressure fluctuations surrounding a turbulent jet, J. Fluid Mech. 340 (1997) 1–33.

[23]A. Cavalieri, D. Rodríguez, P. Jordan, T. Colonius, Y. Gervais, Wavepackets in the velocity field of turbulent jets, submitted to J. Fluid Mech.

[24]M. Lighthill, On sound generated aerodynamically. I. General theory, Proc. R. Soc. Lond. A. 211 (1107) (1952) 564–587.

[25]S. C. Crow, Acoustic gain of a turbulent jet, Vol. 16 of Phys. Soc. Meeting, Colorado, Boulder, 1972.

[26]D. G. Crighton, Basic principles of aerodynamic noise generation, Prog. Aero. Sci. 16 (1975) 31–96.

[27]D. G. Crighton, P. Huerre, Shear-layer pressure fluctuations and superdirective acoustic sources, J. Fluid Mech. 220 (1990) 355–368.

[28]R. Reba, S. Narayanan, T. Colonius, Wave-packet models for large-scale mixing noise, Int. J. Aeroacoustics 9 (2010) 533–558.

[29]T. Colonius, A. Samanta, K. Gudmundsson, Parabolized stability equation models of large-scale jet mixing noise, Procedia Engineering 6 (2010) 64–73.

[30]R. H. Schlinker, J. C. Simonich, R. A. Reba, T. Colonius, K. Gudmundsson, F. Ladeinde, Supersonic jet noise from round and chevron nozzles: Experimental studies, AIAA Paper 2009-3257.

[31]G. A. Brès, J. W. Nichols, S. K. Lele, F. E. Ham, Towards best practices for jet noise predictions with unstructured large eddy simulations, AIAA Paper 2012-2965.

[32]C. A. Brown, J. Bridges, Small hot jet acoustic rig validation, Tech. Rep. NASA TM-2006-214234 (2006).

[33]D. Rodríguez, A. Sinha, G. A. Brès, T. Colonius, Parabolized Stability Equation models in turbulent supersonic jets, AIAA Paper 2012-2117.

[34]T. Herbert, Parabolized stability equations, Annu. Rev. Fuid Mech. 29 (1997) 245–283.

[35]C. Grosch, H. Salwen, The continuous spectrum of the orr-sommerfeld equation. Part I. The spectrum and the eigenfunctions, J. Fluid Mech. 87 (1978) 33–54.

[36]H. Salwen, C. Grosch, The continuous spectrum of the orr-sommerfeld equation. Part II. Eigenfunction expansions, J. Fluid Mech. 104 (1981) 445–465.

[37]D. Rodríguez, A. Sinha, G. A. Brès, T. Colonius, Inlet conditions for wave packet models in turbulent jets based on eigenmode decomposition of les data, Physics of Fluids under revision.

[38]L. Sirovich, Chaotic dynamics of coherent structures. parts i-iii, Quarterly of Applied Math. XLV (3) (1987) 561–582.

[39]J. B. Freund, T. Colonius, POD analysis of sound generation by a turbulent jet, AIAA Paper 2002-0072.

[40]D. Rodríguez, A. V. G. Cavalieri, T. Colonius, P. Jordan, Wavepacket eduction in turbulent jets based on eigenmode decomposition of piv data, 19th AIAA/CEAS Aeroacoustics Conference and Exhibit, 27-29 May, AIAA, Berlin, Germany, 2013.

[41]T. Colonius, J. B. Freund, Application of Lighthill's equation to a Mach 1.92 turbulent jet, AIAA J. 38 (2) (2000) 368–370.

[42]J. Freund, Noise-source turbulence statistics and the noise from a mach 0.9 jet, Physics of Fluids 15 (6) (2003) 1788–1799.

[43]P. Morse, H. Feshbach, Methods of theoretical physics, McGraw-Hill, 1953.

[44]J. Freund, Noise sources in a low reynolds number jet at mach 0.9, J. Fluid Mech. 438 (2001) 277–305.

[45]C. K. W. Tam, T. Chen, Turbulent mixing noise from supersonic jets, AIAA J. 32 (9) (1994) 1774–1780.

[46]D. Rodríguez, A. Samanta, A. Cavalieri, T. Colonius, P. Jordan, Parabolized Stability Equation models for predicting large-scale mixing noise of turbulent round jets, AIAA Paper 2011-2838.

[47]J. W. Nichols, S. K. Lele, Global modes and transient response of a cold supersonic jet, J. Fluid Mech. 669 (2011) 225–241.